

GEMINI DEEP DEEP SURVEY. VI. MASSIVE H δ -STRONG GALAXIES AT $Z \simeq 1$

DAMIEN LE BORGNE¹, ROBERTO ABRAHAM¹, KATHRYNE DANIEL², PATRICK J. MCCARTHY³, KARL GLAZEBROOK², SANDRA SAVAGLIO², DAVID CRAMPTON⁴, STÉPHANIE JUNEAU^{5,4}, RAY G. CARLBERG¹, HSIAO-WEN CHEN^{6,9}, RONALD O. MARZKE⁷, KATHY ROTH⁸, INGER JØRGENSEN⁸, RICHARD MUROWINSKI⁴

Accepted by ApJ, to appear in v640, 20 March 2006

ABSTRACT

We show that there has been a dramatic decline in the abundance of massive galaxies with strong H δ stellar absorption lines from $z \sim 1.2$ to the present. These “H δ -strong”, or HDS, galaxies have undergone a recent and rapid break in their star-formation activity. Combining data from the Gemini Deep Deep and the Sloan Digital Sky Surveys to make mass-matched samples ($M_{\star} > 10^{10.2} M_{\odot}$, with 25 and 50, 255 galaxies, respectively), we find that the fraction of galaxies in an HDS phase has decreased from about 50% at $z = 1.2$ to a few percent today. This decrease in fraction is due to an actual decrease in the number density of massive HDS systems by a factor of 2-4, coupled with an increase in the number density of massive galaxies by ~ 30 percent. We show that this result depends only weakly on the threshold chosen for the H δ equivalent width to define HDS systems (if greater than 4Å) and corresponds to a $(1+z)^{2.5 \pm 0.7}$ evolution. Spectral synthesis studies of the high-redshift population using the PÉGASE code, treating H δ_A , EW[O II], D_n4000 , and rest-frame colors, favor models in which the Balmer absorption features in massive H δ -strong systems are the echoes of intense episodes of star-formation that faded $\simeq 1$ Gyr prior to the epoch of observation. The $z = 1.4 - 2$ epoch appears to correspond to a time at which massive galaxies are in transition from a mode of sustained star formation to a relatively quiescent mode with weak and rare star-formation episodes. We argue that the most likely local descendants of the distant massive HDS galaxies are passively evolving massive galaxies in the field and small groups.

Subject headings: Galaxies: formation — galaxies: evolution — galaxies: high-redshift

1. INTRODUCTION

The history of cosmic star-formation can be conveniently encapsulated by the evolution of the star-formation rate density (SFRD) as a function of redshift z . The SFRD is a fundamental quantity that places stringent limits on models for galaxy formation (e.g. Madau et al. 1998). In hierarchical models, individual galaxies are the ephemeral building blocks of more massive systems, and galaxy formation is a continuous process. In this picture, it is difficult to make an evolutionary connection between a massive galaxy seen at low redshift and a very similar galaxy seen at a substantially higher redshift, because today’s massive galaxies were in several pieces at high redshifts. This difficulty in ‘con-

necting the dots’ between similar galaxies over a range of redshifts is greatly reduced if massive galaxies form earlier and are longer-lived than predicted by early generations of hierarchical models, as now appears to be the case (Glazebrook et al. 2004, hereafter Paper III). In this view, a detailed understanding of the formation and evolution of *individual* massive galaxies is entirely complementary to the study of volume-averaged quantities such as the SFRD (e.g. Juneau et al. 2005, hereafter Paper V).

Broad-band colors and spectral features have long been used to probe the star-formation history of individual galaxies, with mixed success. Emission lines and blue starlight probe the current star-formation rate. Constraints on the past history of star-formation from the colors and spectral features of older stellar populations, however, are hampered by the well-known age-metallicity degeneracy. Fortunately, characterizing the *recent* ($\lesssim 2$ Gyr) star-formation history of galaxies is more tractable. In particular, the H δ_A Lick index (Worthey & Ottaviani 1997) and the 4000-Å break (Dressler & Shectman 1987), when combined together, have proved to be powerful diagnostics for probing recent star-formation. Such subtle diagnostics of recent star-formation can only be probed by spectroscopy as they only have small effects on broad-band colors. Galaxies which have experienced a break in their star-formation history are particularly well identified by such features. For instance, the evolution of the H δ_A Lick index for a stellar population reaches high values (> 5 Å, corresponding to a strong absorption line) only when this population is dominated by A stars, which happens exclusively for intermediate ages (~ 300 Myr to ~ 2 Gyr)

¹ Department of Astronomy & Astrophysics, University of Toronto, Toronto ON, M5S 3H8 Canada, [leborgne; abraham; carlberg]@astro.utoronto.ca

² Department of Physics & Astronomy, Johns Hopkins University, Baltimore, MD 21218, [kdaniel; kgb; savaglio]@pha.jhu.edu

³ Carnegie Observatories, 813 Santa Barbara St, Pasadena, CA 91101, pmc2@ociw.edu

⁴ NRC Herzberg Institute for Astrophysics, 5071 W. Saanich Rd., Victoria, BC, Canada, [david.crampton; murowinski]@nrc-cnrc.gc.ca

⁵ Département de physique, Université de Montréal, 2900, Bld. Édouard-Montpetit, Montréal, QC, Canada H3T 1J4, sjuneau@astro.umontreal.ca

⁶ Center for Space Sciences, Massachusetts Institute of Technology, 70 Vassar St., Bld. 37, Cambridge, MA 02139, hchen@space.mit.edu

⁷ Department of Physics and Astronomy, San Francisco State University, San Francisco, CA 94132, marzke@stars.sfsu.edu

⁸ Gemini Observatory, 670 North A’ohoku Place, Hilo, HI 97620, [jorgensen; kroth]@gemini.edu

⁹ Hubble Fellow

under the condition that no significant star formation has occurred in the last few hundred Myrs. This behavior is predicted with good confidence by the recent generation of galaxy evolution models, such as PÉGASE.2 (Fioc & Rocca-Volmerange 1997, 1999) and PÉGASE-HR (Le Borgne et al. 2004) at low and high spectral resolutions, respectively. The systems identified by this particularly deep H δ line are usually called “H δ -strong”.

The H δ line and the 4000-Å break have long been used to probe stellar populations, originally mostly in clusters of galaxies (Dressler & Gunn 1983; Couch & Sharples 1987; Abraham et al. 1996; Poggianti et al. 1999), and more recently also in field galaxies (Zabludoff et al. 1996; Zabludoff 1999; Balogh et al. 1999; Goto et al. 2003; Quintero et al. 2004; Tran et al. 2004; Yang et al. 2004). In a particularly significant recent development, Kauffmann et al. (2003) have used these features to examine the star formation histories of large samples of local galaxies from the Sloan Digital Sky Survey (SDSS). In the present paper we complement the Kauffmann et al. (2003) work by measuring the same spectral features in distant ($z = 0.6 - 1.2$) galaxies from the Gemini Deep Deep Survey (GDDS, Abraham et al. 2004, hereafter Paper I). Building two unbiased samples of massive ($M_* > 10^{10.2} M_\odot$) galaxies at $z = 0.6 - 1.2$ and $z = 0.05 - 0.1$ from the GDDS and the SDSS, respectively, we investigate the differences in the star-formation histories at these two epochs. Such a comparison can shed light on the evolution of massive galaxies since $z = 2$: the local massive galaxies, dominated by elliptical morphologies, are known to be nearly-passively evolving. Similarly massive galaxies have also been found in surprisingly large numbers at higher redshifts (up to $z = 2$, Paper III, Fontana et al. 2004) and some of these are already “red and dead” (Cimatti et al. 2004; McCarthy et al. 2004, hereafter Paper IV). Our aim is to use spectral features to better understand the detailed star formation histories of these systems.

This paper is organized as follows. Our high-redshift and low-redshift galaxy samples are described in Section 2. Section 3 presents the measurements we have obtained from these data. Results obtained from these measurements are given in Section 4. Modeling and interpretation of our data are presented in Section 5, and our conclusions are given in Section 6. Cosmological parameters $H_0 = 75 \text{ km s}^{-1} \text{ Mpc}^{-1}$, $\Omega_\Lambda = 0.7$, and $\Omega_M = 0.3$ are assumed throughout this paper.

2. SAMPLE SELECTION

The present study is based on two spectroscopic surveys at low and high redshifts. At $z \geq 1.1$, the GDDS contains more than 300 high-quality galaxy spectra and has a very well-understood selection function (Paper I) designed to make it possible to use it as an unbiased mass-limited sample. At low redshift ($z \simeq 0.1$), the SDSS provides many thousands of galaxy spectra with excellent quality. In this Section, we first give a brief overview of the common selection criteria for these two samples, before describing the details of each sample in more detail.

2.1. Overview

Our overall sample is selected from the GDDS and SDSS using three criteria. (1) We restrict our anal-

ysis to galaxies with secure redshifts and high quality spectra. Our threshold corresponds to a typical signal-to-noise ratio of $S/N > 2$ per pixel. (2) Then, we restrict the redshift range of each sample to the maximum interval over which the measurement of both H δ and the 4000-Å break is possible in the data. (3) Finally, we select galaxies with a total stellar mass larger than $10^{10.2} M_\odot$. With this purely physical selection we avoid color selection biases (for instance, UV-selected samples can over-represent star-forming galaxies with respect to red galaxies). We choose this particular mass cut-off because it corresponds to the lowest mass for which the GDDS sample can be considered as complete in the redshift range defined by our second criterion. Doing so, we also maximize the number of galaxies included in the high redshift sample, which makes our results more robust. Finally, given this mass cut-off, we further restrict the SDSS sample to the redshift range over which the survey is complete. Eventually, we obtain two comparable, mass-limited samples at low ($0.05 < z < 0.1$) and high ($0.6 < z < 1.2$) redshifts.

2.2. The GDDS sample

The characteristics of the Gemini Deep Deep Survey are described in Paper I; only a very brief description of the survey is given here. The GDDS targets galaxies in the “redshift desert” ($1 < z < 2$). The survey contains 312 spectra of galaxies in four fields of the Las Campanas Infrared Survey (McCarthy et al. 2001). The primary selection is based on near-infrared photometry ($K_s < 20.6$, $I < 24.5$ in Vega magnitudes) giving preference to galaxies with red $I - K$ colors and photometric redshifts above $z = 1$ (Chen et al. 2002; Firth et al. 2002).

Spectra were obtained with the GMOS multi-slit spectrograph on the Gemini North 8 meter telescope. The “Nod & Shuffle” technique was used to optimize sky subtraction in order to allow very long exposures ($\gtrsim 30$ hours per field) to be undertaken. This yielded high-quality spectra with $\text{FWHM} \simeq 17 \text{ \AA}$ from which spectroscopic redshift determinations were successful for $\simeq 75\%$ of the sample. About 80% of the galaxies with secure redshift also satisfy the condition $S/N > 2$ per pixel around the H δ line.

In this paper our sample is restricted to the 62 galaxies with high-quality spectra and secure redshifts in the range $0.6 < z < 1.2$. This range corresponds to the maximum interval over which all galaxies have measurable H δ_A and D_n4000 indices. We further limit the sample to galaxies with stellar masses $M_* > 10^{10.2} M_\odot$, leading to a subsample of 26 galaxies. The choice of this mass cut-off maximizes the number of galaxies in our GDDS sample (it is the minimum mass for which our sample is mass-complete over the redshift range $0.6 < z < 1.2$, as demonstrated in Paper III). Stellar masses, derived from template fits to the multicolor (VIK) photometry, are taken from Paper III. The masses used in this paper assume a Baldry & Glazebrook (2003) Initial Mass Function (hereafter BG03 IMF). The typical error bar on $\log_{10} M_*$, estimated by Monte Carlo simulations, is of the order of 0.2 dex. A single galaxy (GDDS-02-2197) is then removed from this subsample because of very doubtful measured H δ_A and D_n4000 indices. This galaxy is an outlier with the largest error bars in the sample. In fact, these error bars are so large that the object is compatible

TABLE 1
 PROPERTIES OF OUR SAMPLE OF GDDS MASSIVE GALAXIES.

ID	z	H δ_{A} (\AA)	EW[O II] (\AA)	D_n4000	$\log_{10}(M_*/M_{\odot})$	$g - r$	SFR([OIII]) ($M_{\odot}\text{yr}^{-1}$)	M_*/SFR (Gyr)	weight
GDDS-22-2863	0.918	11.81 \pm 4.10	-47.58 \pm 8.72	1.16 \pm 0.11	10.30 \pm 0.30	0.62	1.7	11.6	0.070
GDDS-22-0128	1.024	11.62 \pm 2.65	-56.41 \pm 12.69	1.49 \pm 0.13	10.55 \pm 0.28	0.60	1.7	20.7	0.028
GDDS-12-8139	1.189	8.36 \pm 0.54	-6.21 \pm 0.65	1.61 \pm 0.02	10.39 \pm 0.29	0.40	2.3	10.5	0.019
GDDS-02-1724	0.996	7.58 \pm 0.19	-2.45 \pm 0.32	1.34 \pm 0.01	10.87 \pm 0.09	0.37	2.6	27.7	0.007
GDDS-12-5722	0.841	6.14 \pm 0.58	-8.74 \pm 1.11	1.34 \pm 0.02	10.69 \pm 0.10	0.67	1.6	31.1	0.166
GDDS-22-0281	1.022	6.10 \pm 1.26	-14.88 \pm 2.31	1.60 \pm 0.06	11.02 \pm 0.13	0.71	1.5	70.6	0.166
GDDS-02-1777	0.982	4.74 \pm 0.90	-10.81 \pm 1.71	1.31 \pm 0.03	10.43 \pm 0.22	0.56	2.3	11.5	0.033
GDDS-02-1702	1.052	4.58 \pm 1.58	-42.99 \pm 2.42	1.17 \pm 0.04	10.40 \pm 0.18	0.33	9.0	2.8	0.020
GDDS-02-1543	1.131	4.22 \pm 2.65	-5.34 \pm 2.71	1.28 \pm 0.06	10.80 \pm 0.15	0.67	0.2	267.4	0.070
GDDS-22-2548	1.022	3.47 \pm 1.51	-17.08 \pm 2.46	1.71 \pm 0.07	10.99 \pm 0.18	0.70	2.3	41.5	0.166
GDDS-22-0315	0.909	3.13 \pm 0.96	-14.90 \pm 1.05	1.56 \pm 0.03	10.69 \pm 0.10	0.53	4.2	11.7	0.013
GDDS-12-7660	0.791	3.04 \pm 0.79	-15.66 \pm 1.11	1.20 \pm 0.02	10.48 \pm 0.14	0.46	2.5	12.3	0.013
GDDS-02-0715	1.133	3.01 \pm 2.14	-4.29 \pm 2.22	1.35 \pm 0.06	11.25 \pm 0.06	0.37	1.8	101.6	0.053
GDDS-15-6851	1.126	3.00 \pm 0.92	-8.32 \pm 1.51	1.64 \pm 0.03	10.68 \pm 0.13	0.62	4.2	11.5	0.028
GDDS-12-5337	0.679	2.30 \pm 0.39	-13.30 \pm 1.17	1.67 \pm 0.02	10.42 \pm 0.13	0.50	1.9	14.0	0.027
GDDS-12-8983	0.963	0.72 \pm 0.34	-1.51 \pm 0.50	1.77 \pm 0.02	10.70 \pm 0.07	0.56	0.6	89.7	0.015
GDDS-22-0893	0.875	0.34 \pm 1.38	-6.52 \pm 1.81	1.93 \pm 0.07	10.59 \pm 0.18	0.68	0.6	60.2	0.033
GDDS-02-0857	1.049	0.13 \pm 1.23	-6.51 \pm 1.28	1.88 \pm 0.05	11.21 \pm 0.06	0.79	1.8	87.1	0.168
GDDS-12-6800	0.615	-0.13 \pm 0.34	0.95 \pm 0.64	2.03 \pm 0.02	10.89 \pm 0.09	0.73	0.1	1443.0	0.038
GDDS-12-6456	0.612	-0.43 \pm 0.57	-0.06 \pm 1.08	1.99 \pm 0.04	10.72 \pm 0.14	0.73	0.2	286.3	0.027
GDDS-02-1011	1.133	-1.04 \pm 2.00	4.93 \pm 1.53	1.78 \pm 0.07	10.48 \pm 0.13	0.65	0.3	88.8	0.070
GDDS-02-1935	0.915	-1.12 \pm 2.84	-4.28 \pm 2.84	1.82 \pm 0.10	11.12 \pm 0.07	0.77	0.4	336.7	0.166
GDDS-15-5348	0.964	-1.97 \pm 1.19	-10.82 \pm 3.55	1.96 \pm 0.07	11.06 \pm 0.07	0.71	0.8	149.1	0.166
GDDS-15-7241	0.749	-2.29 \pm 0.68	-1.30 \pm 0.98	1.74 \pm 0.03	10.70 \pm 0.14	0.62	0.2	260.4	0.011
GDDS-22-0510	0.820	-2.30 \pm 1.13	-2.63 \pm 1.34	1.81 \pm 0.04	10.51 \pm 0.13	0.67	0.6	55.0	0.013

with the rest of the sample in a formal statistical sense, so simply omitting it changes none of our conclusions while simplifying the analysis. This leaves us with 25 galaxies in the final GDDS subsample. The main properties of these 25 galaxies are given in Table 1. A full description of all the measured quantities present in this table is given in Section 3.

Figure 1 presents rest-frame spectra of all 25 GDDS galaxies investigated in the present paper, with a 3-pixel boxcar smoothing, together with the error spectra (in blue) and their ACS HST images (see also Abraham et al. 2005) when available. The color of the frame around each image codes the spectral classification of the galaxy (Table 5 of Paper I, red for old stellar populations, green for intermediate age and blue for young stellar populations). The median redshift of this sample is $\bar{z} = 0.964$.

The selection function for the GDDS is given in Paper I. The inverse weights in that paper quantify the degree to which each galaxy is over-represented in a $I - K$ vs. I color-magnitude diagram. It is important to note that the primary goal of the GDDS survey was to study red galaxies at high redshift. Therefore, by design, this survey specifically targeted red galaxies with a sparse sampling rate of $\sim 1/2$ compared to $\sim 1/7$ for the remainder of the photometric sample. The inverse weights must therefore be used to account for this unbalance. As we have just described in Section 2.1, in the present paper further restrictions on the sample are introduced (so as to only include galaxies with high confidence redshift class and high spectral quality), and a new set of weights is needed to define the selection function for this sample.

These are given in the last column Table 1¹⁰. In Section 4, we will show that our results are not strongly dependent on the adopted weights.

2.3. The SDSS sample ($\bar{z} \simeq 0.1$)

At low redshift, we define a sample of galaxies drawn from the Sloan Digital Sky Survey DR2 (Abazajian et al. 2004). We restrict the present investigation to the ‘main’ galaxy sample, i.e. galaxies with Petrosian r -band magnitudes in the range $14.5 < r < 17.77$. Only galaxies with secure redshift measurements are considered. To reduce sampling incompleteness, we focus on galaxies with $z > 0.05$, and in order to be consistent with the quality of the GDDS spectra, we also exclude the few galaxies (0.2% of the sample) with $S/N < 2$.

As for the GDDS sample, we also impose a mass cut, so that our sample includes only massive galaxies ($M_* > 10^{10.2} M_{\odot}$). According to the SDSS stellar mass function determined by Panter et al. (2004), the sample is complete for $\log_{10}(M_*/h^{-2}) \geq 10.2$ only at $z < 0.1$. Using the cosmology adopted in our study, this corresponds to $M_* \geq 10^{9.9} M_{\odot}$. However, this mass-function is estimated using a Salpeter (1955) IMF, while the stellar masses of GDDS galaxies are estimated using the BG03 IMF. The conversion factor between these mass estimates is $M_{\text{SP}} = 1.82 M_{\text{BG}}$ (Paper III), or 0.26 dex. Including this correction, we consider that the SDSS sample is complete for $M_* > 10^{10.2} M_{\odot}$ (using the BG03 IMF) for $z < 0.1$. We use the mass estimates from Kauffmann et al. (2003) which are corrected from dust-obscuration. Because these authors use a Kroupa (2001)

¹⁰ We emphasize that these are *inverse* weights. A small number implies that the object needs to be weighted more heavily because it is under-represented in the sample.

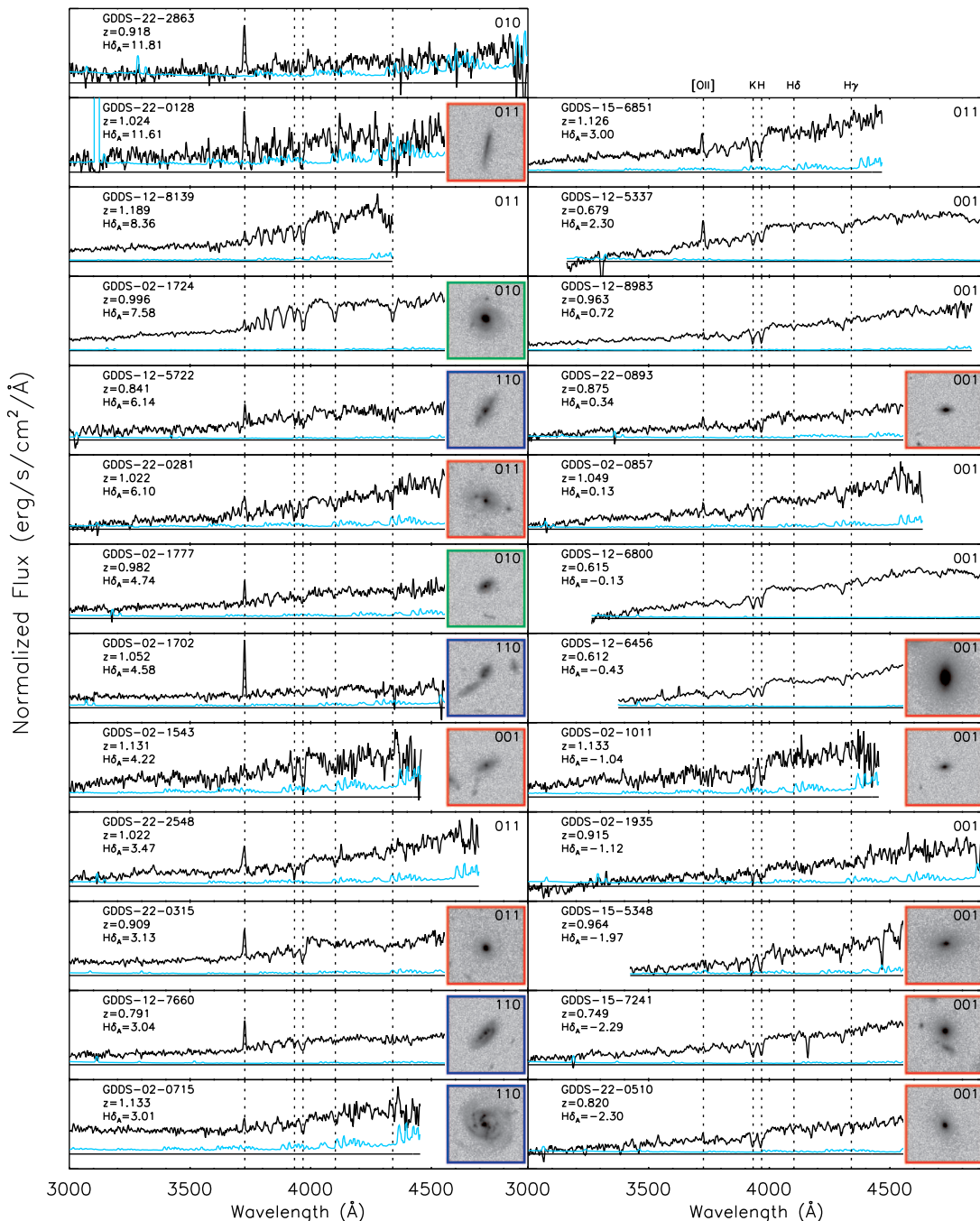


FIG. 1.— Sample of the 25 mass selected GDDS galaxies, sorted by decreasing $H\delta_A$ (expressed in \AA). The error spectra are in blue and HST ACS images are shown when available. The size of these images is 5×5 arcsec 2 . The color of the frame around each image codes the luminosity-mean age of the galaxy (estimated by visual inspection of the spectrum and broad-band SED, cf Paper I): red for old stellar populations (codes 001 and 011), green for intermediate age (code 101) and blue for young stellar populations (code 110). Note that slightly negative values for $H\delta_A$ ($\lesssim 3\text{\AA}$) do not necessarily correspond to emission lines (e.g. GDDS-15-7241), because of the very definition of this Lick index: even when the $H\delta$ line is in absorption, the pseudo-continuum can be “lower” than the line itself.

IMF, we subtract 0.07 dex from their masses to convert to BG03 IMF mass estimates. For our subsample of SDSS galaxies, the typical 95% confidence range on $\log M_*$ is 0.2 dex.

After imposing the cuts described above, our final SDSS low-redshift sample contains 50, 255 galaxies.

3. MEASUREMENTS

In this Section, we provide a detailed description of the quantities measured from our low-redshift and high-redshift samples. The reader who is not interested in details of how these measurements were made may wish to simply note that we measured a single rest-frame broad-band color and the spectral indices listed in Table 2, and then move ahead to Section 5.

TABLE 2
DEFINITIONS OF THE SPECTRAL INDICES USED IN THIS PAPER.

Index	Blue band (\AA)	Feature band (\AA)	Red band (\AA)
D_n4000	3850.00-3950.00		4000.00-4100.00
$H\delta_A$	4042.85-4081.00	4084.75-4123.50	4129.75-4162.25
EW($H\delta$)	4017.00-4057.00	4083.50-4122.25	4153.00-4193.00
EW[O II]	3696.30-3716.30	3716.30-3738.30	3738.30-3758.30

3.1. Rest-frame $g-r$ color

At low redshift, SDSS galaxy spectra and fiber u,g,r,i,z magnitudes are publicly available. However, given that we use the SDSS spectra to measure other spectral indices (D_n4000 and $H\delta_A$), we decided to measure a color directly on the SDSS spectra to be consistent in our measurements (and to avoid, for example, aperture effects which might affect differently the spectral features and the photometry). Because of this choice, $g-r$ and $B-V$ are the two main optical colors available for the SDSS galaxies. We checked that both colors give similar results, and we concentrate on the $g-r$ color in the following. The $g-r$ color is measurable on 95% of the SDSS spectra.

Unfortunately, because of the limited wavelength coverage of the GDDS galaxy spectra, it is not possible to measure a standard optical color from them in the same way. At redshift $\simeq 1.1$, the optical spectra of the GDDS galaxies correspond to UV rest-frame spectra. However, the existence of optical and near-infrared photometry makes it possible to estimate a rest-frame optical color, using k -corrections, in the following way. The rest-frame $g-r$ color of the GDDS galaxies was measured on the synthetic spectra that fit best the observed spectral energy distributions, using the B,V,R,I,z,J,H and K photometry. The procedure used to fit the data combines two instantaneous bursts of star formation at different ages and metallicities, reddened by dust (parameterized by $E(B-V)$, ranging from 0 to 2). A minimization of the χ^2 using the ages, the metallicities and the extinction as free parameters, provides a best-fitting synthetic spectrum. (It is worth mentioning that this procedure was not used to derive ages, metallicities, or extinction parameters: doing so would require a much more refined grid than the one we used because of the degeneracies that exist in the measurement of these three parameters.) Column 8 of Table 1 lists the measurements of the $g-r$ color for the GDDS galaxies in our sample.

3.2. D_n4000

The $g-r$ color of a galaxy can be affected by the presence of dust, and the D_n4000 at 4000 \AA is often used to estimate ages instead because it is much less sensitive to extinction. For example, a reddening of $E(B-V)=0.5$ shifts D_n4000 by less than 10 percent, which is of the order of the change produced by a relative difference in age of 0.25 dex (or $\simeq 45\%$). This effect is small in comparison to the corresponding reddening of the $g-r$ color, which can be mistaken for a $\simeq 1$ dex age effect. Remarkably, the dependence of D_n4000 on the metallicity is much stronger than its dependence on the extinction: for a 10 Gyr old population, it varies from 1.7 to 2.7 when the metallicity varies from $Z_\odot/5$ to $2.5Z_\odot$ (e.g.

Kauffmann et al. 2003). The definition of D_n4000 (from Balogh et al. 1999) is reported in Table 2 together with the other indices used in this paper.

3.3. The $H\delta$ line

In the absence of emission, the equivalent widths of Balmer absorption lines decrease steadily with time for an old (age > 1 Gyr) passively evolving stellar population. Moreover, they are quite generally little to the mean stellar metallicity and dust content of a galaxy. However, in practice, $H\alpha$ and $H\beta$ are often partially filled in by nebular emission, making their interpretation more difficult. Very high order lines are generally too weak to be easily measurable, so $H\gamma$ and $H\delta$ are the two lines of choice for probing stellar ages. In the present study we concentrate on $H\delta$ because, unlike the lower order Balmer lines, it is measurable in optical spectra of galaxies redshifted up to $z = 1.2$.

An interesting property of the $H\delta$ absorption line lies in its behavior between the birth of a generation of stars and the age of 2 Gyr: the equivalent width first increases strongly during a few 10^8 years, reaches its maximum value (almost 10 \AA) when the population is dominated by A stars, and then decreases continuously, passing through its initial value when the population is about 2 Gyr old. This behavior implies that high equivalent widths in absorption ($\gtrsim 4 \text{\AA}$) can only be reached in galaxies where some substantial star formation occurred a few 10^8 years before, and where the subsequent star formation events were weak. We will refer to systems with $H\delta_A > 4 \text{\AA}$ as being “ $H\delta$ -strong” (HDS).

To measure the equivalent width of $H\delta$, we use the definition of the Lick index $H\delta_A$ (Worthey & Ottaviani 1997) which is well suited to probe stellar populations dominated by A stars in the optical. We degrade the resolution of all the rest-frame spectra to the appropriate Lick resolution (11 \AA), following the prescription of Worthey & Ottaviani (1997).

For the sake of consistency between the two data sets, we choose to measure the $H\delta_A$ and D_n4000 indices ourselves on the SDSS spectra, rather than using the previously published values. To validate these measurements, we compare them with the values published by Kauffmann et al. (2003, hereafter K03) in Fig. 2. Perfect agreement is not expected: the differences between our measurements of $H\delta_A$ and the values given by K03 can be partly explained by the different spectral resolutions ($\simeq 3 \text{\AA}$ for K03, and $\simeq 11 \text{\AA}$ for this work which uses the Lick resolution). Moreover, unlike those authors, we choose not to correct $H\delta_A$ from the nebular emission for two reasons: first, we prefer to compare the raw data to models that include the contribution from emission lines; second, the correction from the contribution from emission lines to the $H\delta_A$ index is too uncertain for the GDDS galaxies which have on average lower S/N ratios than the SDSS spectra. However, the agreement between the two measurements is good, given the different considerations involved in the measurements. For large values of $H\delta_A$, our measured values are smaller than the K03 values by $\simeq 1 \text{\AA}$. This is to be expected as a correction for line emission in such young populations would increase $H\delta_A$ by about 1 – 3 \AA , as predicted by the PÉGAISE models. A similar correction is mentioned in Balogh et al. (1999), and is confirmed by Goto et al. (2003) who measured a

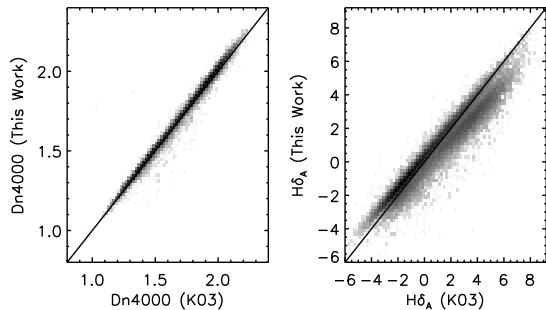


FIG. 2.— Comparison of D_n4000 and $H\delta_A$ measurements on our SDSS sample between Kauffmann et al. (2003) (with a correction for nebular emission and a higher spectral resolution) and this work (including the emission lines and at the Lick spectral resolution). The grey scale level represent the number of galaxies in each pixel in a logarithmic scale, darker pixels having more galaxies.

median correction of 15% for the $H\delta$ equivalent width on a sample of galaxies drawn from the SDSS.

3.4. Emission lines

The nebular emission lines produced in H II regions are excellent indicators of recent star-formation. In the redshift range of the GDDS sample, the main visible lines are $[OII]\lambda 3727$ and the $H\delta$ Balmer line ($H\gamma$ and $H\beta$ are too much redshifted to be visible). In the following, we concentrate on the equivalent width of the $[OII]\lambda 3727$ line as an indicator of ongoing or very recent (less than 50 Myr) star formation.

3.5. Errors

The uncertainties on the measurements of $H\delta_A$ and D_n4000 , and $EW[O II]$, reported in Table 1, are computed following Cardiel et al. (1998), using, for each galaxy, the measured mean signal-to-noise ratios inside the integration bands of Table 2. To confirm these error bars, Monte-Carlo simulations were carried out assuming a Gaussian distribution for the error spectrum. For each galaxy, 50 simulations were considered, and the rms dispersion of the distribution of indices matches very well the error bars predicted using the formulae from Cardiel et al. (1998): the rms for the distribution of relative differences between these two errors is 0.22 for $H\delta_A$ and 0.12 for D_n4000 .

Although we believe that the observed fractions of HDS galaxies in each redshift range are robust, several potential sources of errors should first be considered.

The very definitions of the indices used might be a source of systematic errors. We confirmed that the use of the $EW(H\delta)$ definition instead of the index $H\delta_A$ does not change any of our conclusions.

Some errors may also come from the calibration of the original data. In particular, the reddest end of the GDDS spectra is known to be subject to a quite uncertain correction (the "redfix" correction, cf. Paper I) due to charge diffusion in the CCD detectors in the red. Fortunately, this correction applies to the portion of the rest-frame spectrum which contains the $H\delta$ line only at redshifts larger than 1.3. Therefore, it does not affect our study. The selection function, which introduces important weighting, might also be a concern. However, our results are qualitatively the same if this selection function

is omitted. Finally, we estimate that the aperture effects, which could potentially affect the observed integrated spectral indices and colors, are small on average. Indeed, as GDDS galaxies are observed at higher and higher redshift, a larger fraction of the galaxies is enclosed in the $0.75''$ aperture slit (corresponding to a physical diameter of 4.7 kpc at $z = 0.6$ and 5.8 kpc at $z = 1.2$), and more light from the outer parts contributes to the integrated indices. However, over the whole $0.6 < z < 1.2$ interval, a larger fraction of the total light is measured than that measured by the SDSS fibers on the $z = 0.05 - 0.1$ galaxies. The recent work of Brinchmann et al. (2004) and Kewley et al. (2004) showed that aperture effects for emission-line-derived SFR in the SDSS galaxies is negligible for $z > 0.05$. The aperture effects on the stellar absorption lines (typically more concentrated than the emission-lines) are expected to be negligible.

Overall, the main sources of uncertainties are unlikely to explain the observed trend of the decrease of the fraction of HDS galaxies since $z = 1.2$ described in next Section. We conclude that this evolution must be real and can only be explained by changes in the star formation histories of massive galaxies during the past 10 Gyr.

4. COMPARED PROPERTIES OF LOCAL AND DISTANT MASSIVE GALAXIES

4.1. General results

Measurements of the colors and spectral features in the galaxies in our GDDS sample are presented in Table 1. Figures 3 and 4 show the distributions of $H\delta_A$, D_n4000 , and $g - r$ rest-frame color as a function of redshift. In these figures, GDDS galaxies categorized as $H\delta$ -strong ($H\delta_A \geq 4 \text{ \AA}$) are denoted with open circles, and the remaining galaxies of the GDDS sample are shown as filled circles. In addition, these figures show two-dimensionally binned distributions (for both the GDDS sample and the SDSS sample) using colored cells. The reddest (or darkest) cells contain the largest number of galaxies. The size of the cells is chosen to be on the order of, or larger than, the typical error bar of the various observed quantities. The density of GDDS galaxies in each binned cell has been corrected using the weights given in Table 1, and Monte-Carlo simulations of each GDDS galaxy were used to estimate the true distributions shown in these figures. (Note that this explains why the spread data in the color-coded cells is a little larger than the coverage of the individual points). Each of these figures also shows evolutionary models which will be described in the next section.

A comparison of the distributions of the GDDS and SDSS samples in these figures shows a number of interesting results. The most striking difference between the low-redshift and the high-redshift samples is the disproportionately large number of $H\delta$ -strong systems at $z \sim 1$ in the GDDS sample, clearly visible in Figure 3.

To quantify this observation, we measure the number space densities (per comoving Mpc^3) of massive galaxies and massive HDS galaxies in various redshift intervals. For GDDS galaxies ($0.8 \leq z < 1$ and $1 \leq z < 1.2$), we use the sampling weights defined above and the $1/V_{max}$ formalism (Schmidt 1968) to correct from the fact that the faintest galaxies in our sample could not be observed if they were at higher redshift. At low redshift, we use the SDSS sample and the V_{max} values from Blanton et al.

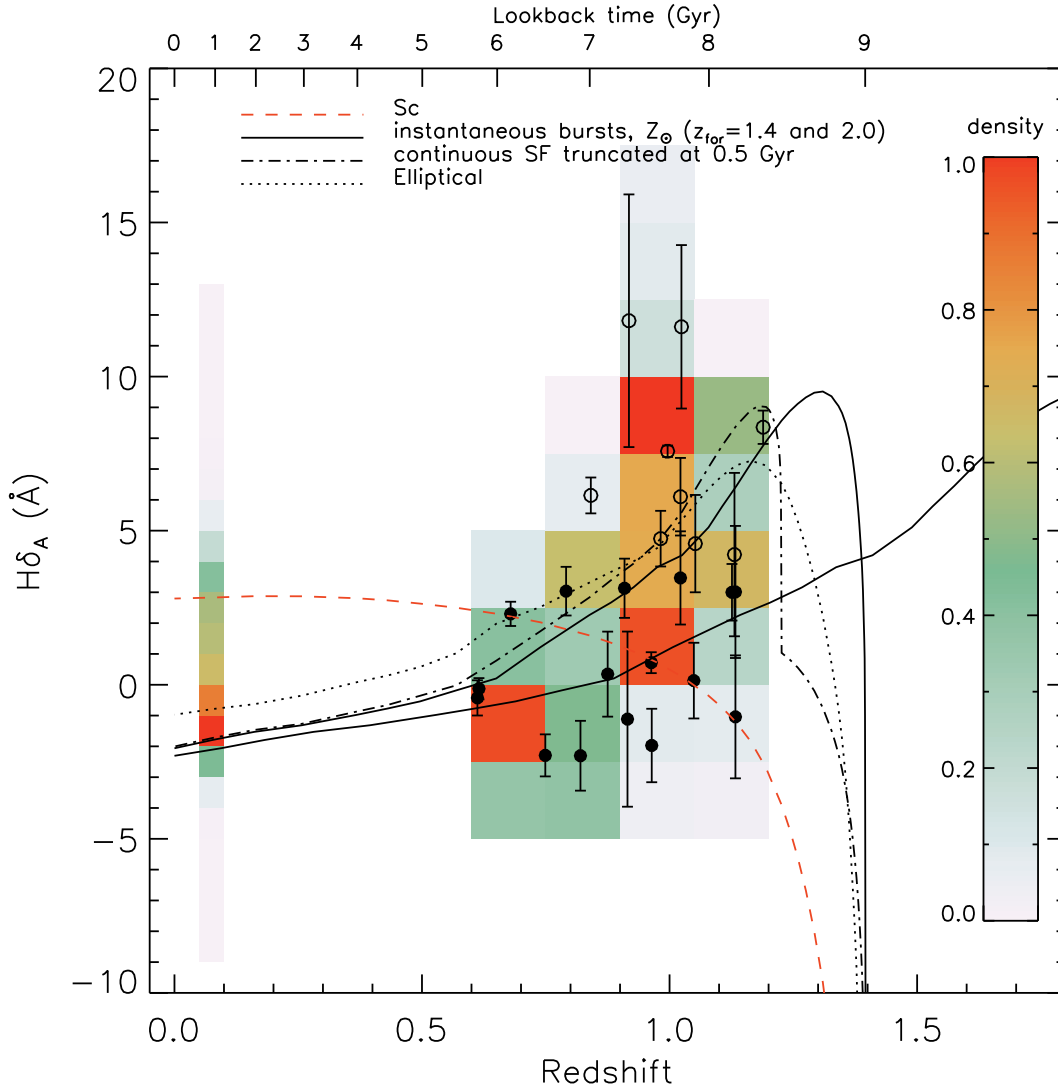


FIG. 3.— Evolution of the $H\delta_A$ index from $z = 1.2$ (GDDS sample) to the present (SDSS sample). For each sample, the plane is gridded and the number of galaxies that can be counted in each cell (we call this quantity “density”) is color-coded: a density of 1 (reddest or darkest color) is assigned to the cell containing the most objects. The GDDS densities are converted from raw number counts by using the selection function and Monte Carlo simulations. The GDDS individual galaxies are represented by filled ($H\delta_A \leq 4 \text{ \AA}$) and empty ($H\delta_A > 4 \text{ \AA}$) circles. The models described in Section 5 are over-plotted: “burst” mode models are represented by black lines and “quiescent” mode models by red lines. The two ‘cycle’ models plotted in the following figures are omitted here for clarity: they would blur the figure, because their $H\delta_A$ indices alternatively reach very positive (when star-formation has ceased) and very negative values (because of emission lines) on short time-scales.

(2003). At every redshift, we treat separately the population of HDS galaxies, defined by $H\delta_A \geq 4 \text{ \AA}$. Figure 5 shows the evolution of the number densities and mass densities from $z \approx 1$ to $z \approx 0$ for massive galaxies ($M_\star > 10^{10.2} M_\odot$ with the BG03 IMF). In particular, it shows that the $z \approx 1$ massive galaxies are about one third (in number) of the local massive galaxies. This means that the GDDS galaxies in our sample are almost certainly progenitors of some of the local massive galaxies (because the stellar mass is expected to either increase or keep steady), but about two thirds of the local massive galaxies had progenitors at $z \approx 1$ that were not massive enough to pass the mass threshold of $M_\star > 10^{10.2} M_\odot$. The figure also confirms previous results (Glazebrook et al. 2004; Fontana et al. 2004), showing that the total stellar mass contained in mas-

sive galaxies at in $z \approx 1$ is already about a third of its present-day value. It is more difficult to link this result with the claim of Bell et al. (2004) that the stellar mass in red galaxies must have doubled since $z = 1$. Indeed, our mass-selected sample contains not only galaxies on the red-sequence, but also star-forming galaxies (see Table 1). Moreover, the mass cut-off adopted here probably excludes the faint-end of the red-sequence at $z \approx 1$.

It also appears for the first time that although the number and mass densities of all massive galaxies both increase by a factor of 2-3 from $z = 1$ to $z = 0$, these densities follow the opposite trend for HDS massive systems: they actually decrease by a factor of 2-4 (for number densities) and 2-7 (for mass densities) during the same period. As a result, the fraction of massive HDS galaxies is indeed much higher at $z \approx 1$ ($\simeq 1/2$) than at $z \approx 0$ (less

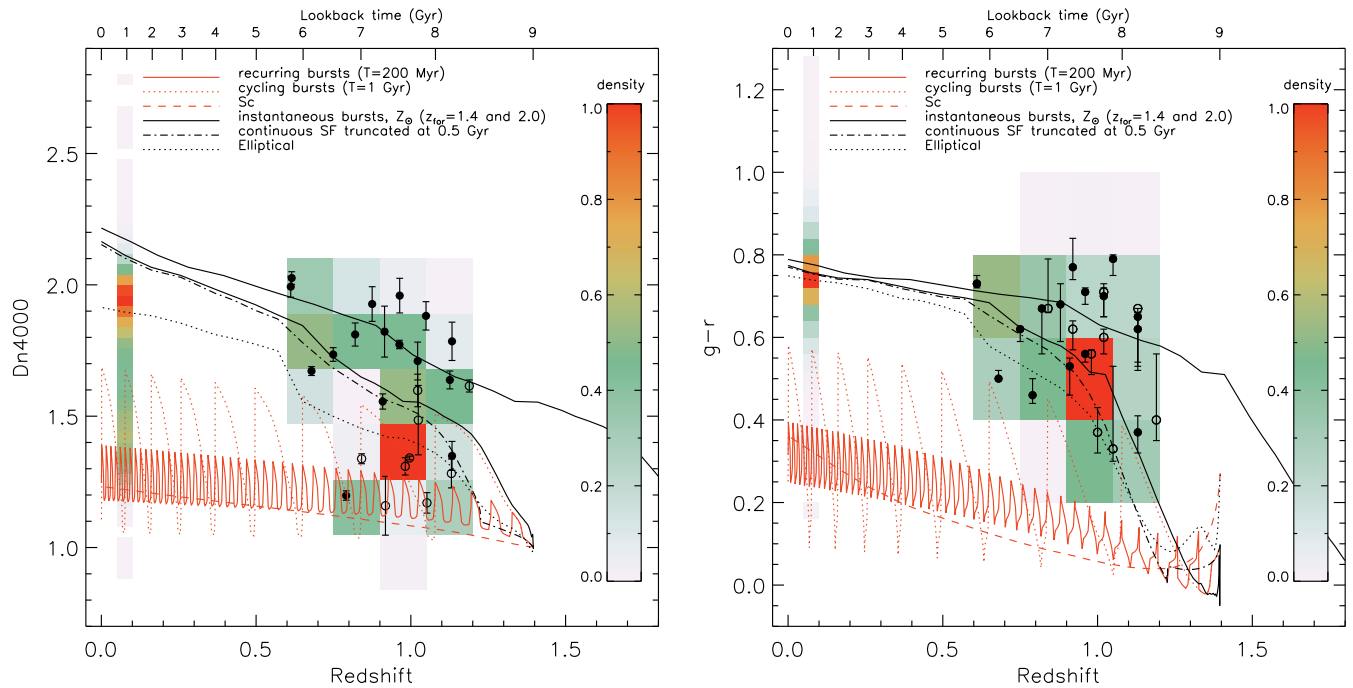


FIG. 4.— Similar to Fig. 3 but for two other tracers of the luminosity-weighted age of galaxies: D_n4000 and the $g-r$ rest-frame color. Symbols as in Fig. 3.

than 1/10). A direct consequence of this strong decrease of number densities for HDS galaxies is that most of the $z = 1$ HDS massive galaxies necessarily end up in local non-HDS (and probably passively evolving) galaxies. This disconnect between distant and local HDS galaxies is not too surprising because the timescales involved are quite different: less than 1-2 Gyr for the HDS phase and ~ 7 Gyr for the Hubble time interval between these two redshifts.

In the second part of this section we will consider how best to parameterize this evolution, and explore the extent to which the evolution depends on the equivalent width threshold beyond which galaxies become flagged as HDS systems.

The comparison of SDSS and GDDS samples in Figure 4 shows complementary information. The non-HDS GDDS galaxies (black dots) tend to have D_n4000 indices almost as large as the values observed at low redshift, whereas the HDS galaxies (empty circles) have a smaller D_n4000 index betraying a smaller luminosity-weighted age. This distinction between HDS and non-HDS galaxies is much less clear for the $g-r$ rest-frame color (right panel of Fig. 4), which can be attributed to differences in extinction by dust. However, over the redshift interval explored by this paper, the GDDS sample is bluer overall than the SDSS sample.

Figure 6 shows, for each sample, the correlation between $H\delta_A$ and D_n4000 . As will be described in the next section, the distributions shown in this figure clearly demonstrate that both the SDSS and GDDS samples of massive galaxies can be divided into two categories: old evolved galaxies with a large D_n4000 break and a small $H\delta_A$ index, and galaxies dominated by younger stellar populations, with a smaller D_n4000 break betraying some recent star formation activity. The well-known

bimodality in the properties of blue and red populations of SDSS galaxies (e.g. Baldry et al. 2004) is only faintly visible in the left panel of this figure; bimodality is not particularly striking in our data because our mass selection isolates the reddest part of the bimodal distribution. Both SDSS and GDDS samples of massive galaxies contain a large fraction of old, passively evolved galaxies (the reddest cells in Figure 6). It is once again seen that, amongst galaxies that have recently formed stars ($D_n4000 < 1.5$), the fraction of HDS galaxies is larger in the GDDS than in the SDSS. Another interesting inference regarding the physical properties of the HDS massive galaxies can be drawn from Figure 6: most of the HDS galaxies seem dominated by young stellar populations (they all have a small D_n4000 break).

Figure 7 presents correlations between $H\delta_A$ and $g-r$ rest-frame color. Most of the HDS objects have redder $g-r$ colors than predicted from passively evolving models (which include no or very little dust). This suggests that massive HDS galaxies, from $z = 1$ to the present, share a common property: they are considerably more reddened by dust ($E(B-V) = 0.2-0.5$) than evolved galaxies. This inference is perhaps not too surprising: having experienced recent episodes of intense star formation, they are more likely to be dusty. This property is confirmed by a two-dimensional KS test, implemented as in Fasano & Franceschini (1987). The two-dimensional statistic D is 0.9, and a Monte-Carlo simulation ensures, at a $> 99.9\%$ confidence level, that the data is not consistent with dust-free models of HDS galaxies. This conclusion is in good agreement with Shioya et al. (2004) who suggest an $A_V > 0.5$ mag extinction in the red HDS systems. It is worth noting that the effect of dust on the spectral indices is very weak: our tests show that $E(B-$

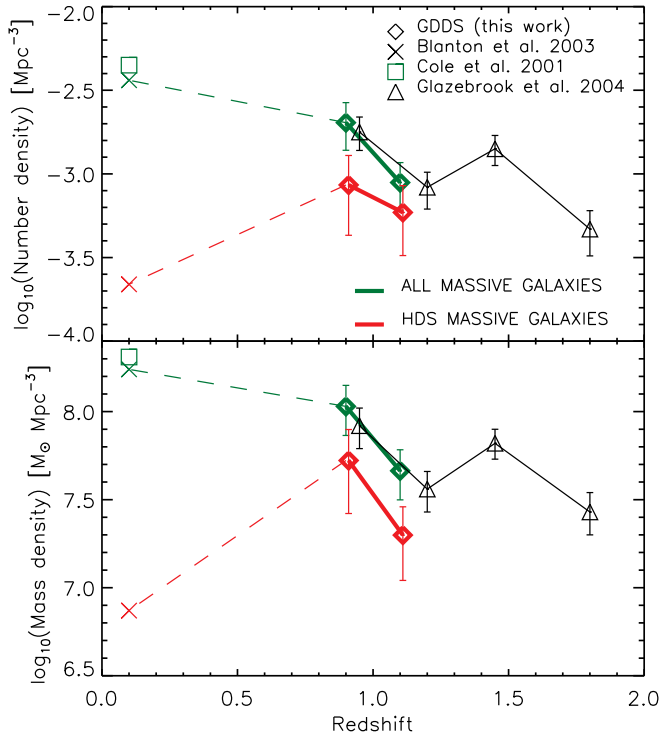


FIG. 5.— Evolution of the number and mass densities of massive galaxies and massive HDS ($H\delta_A > 4\text{\AA}$) galaxies. All these measurements concern only galaxies more massive than $M_* > 10^{10.2} M_\odot$. Sampling weights are applied to GDDS galaxies, and the $1/V_{max}$ formalism is used at every redshift. Poisson error bars are shown for the $z \approx 1$ GDDS galaxies. These are too small to be shown for the $z \approx 0$ samples. Densities at low redshift were taken from Blanton et al. (2003) (from SDSS data, crosses) and Cole et al. (2001) (from 2dF data, squares), and corrected for the same IMF and cosmology. Mass densities from Paper III (Glazebrook et al. 2004) are shown in the lower panel for reference with a black solid line; the corresponding number densities are shown in the upper panel. The high redshift (GDDS) and low redshift (SDSS) samples used in this study are linked with dashed lines.

$V)=0.5$ would not increase $H\delta_A$ by more than 0.2\AA and $D_n 4000$ by more than 10 percent.

4.2. Evolution of the fraction of HDS systems

Figure 5 presented evidence for a differential evolution, from $z = 1.2$ to the present, of the number and stellar mass densities of HDS massive galaxies with respect to populations of massive galaxies. This evolution can also be measured and parameterized more simply through the fraction f_{HDS} of HDS galaxies in unbiased samples of massive galaxies at various redshifts.

Figure 8 presents the evolution of this fraction and clearly shows a steady increase of f_{HDS} with look-back time, going from $f_{\text{HDS}} = 0.01 - 0.2$ in the local universe to $f_{\text{HDS}} \simeq 0.4 - 0.8$ at $z = 1.2$. The different panels in this figure illustrate cases where the $H\delta_A$ threshold (used to define HDS systems) is $H\delta_{A \text{ min}} = 3, 4, \text{ and } 5.5 \text{\AA}$, and show that the measured fraction of HDS systems increases markedly in all cases. In this section, we propose ourselves to parameterize this evolution as a function of the look-back time *and* as a function of the threshold $H\delta_{A \text{ min}}$.

But first, it is worth investigating how sensitive this basic result is to the underlying sample selection func-

tions of the SDSS and GDDS. To investigate this, we explore the effect of the different selection functions applied to the datasets. For the SDSS sample, which is effectively complete, we can simply measure the fraction of HDS galaxies in a single small redshift bin: $0.05 < z < 0.1$. For the GDDS sample, we define three redshift bins with $\Delta z = 0.2$ between $z = 0.6$ and $z = 1.2$ and we measure the fraction of HDS galaxies in each bin, weighting the contribution from each individual galaxy by the sampling weights listed in Table 1. In effect, each galaxy is treated as if it were “1/weight” galaxies. The effect of applying these weights on the measured f_{HDS} , and of ignoring them completely, can be assessed by comparing the diamonds and circles in Figure 8. Clearly the effect of the weighting by the selection function is modest. This is probably due to the fact that the vast majority (23/25) of the massive galaxies in our sample have an observed I-K color greater than 3 magnitudes and lie in a region of the I vs I-K diagram where the GDDS sampling efficiency is fairly high (cf Fig. 12 and 13 of Paper I: about half of the red galaxies were targeted and a redshift could be measured for most of them).

It is worth noting that the error bars on the points shown in Figure 8 cannot be properly described by strict Poissonian statistics, because the quantities plotted are ratios. Instead, we compute the uncertainties following the method of Paterno (2004) which is based on the application of the Bayes’ Theorem to binomial statistics. This method gives realistic errors even when the total number of galaxies inside a bin is very small (and the error on the ratios computed via Poisson errors break down), and when the fraction is close to 0 or 1 (where strict binomial errors break down). We choose to represent the shortest 68.3% confidence interval¹¹. Another precaution is necessary: because the error bars for the $H\delta_A$ index are quite large for the GDDS sample, some galaxies near the limit adopted for $H\delta_A$ could be considered as HDS or not. To quantify this effect, we again made a Monte-Carlo simulation for each galaxy, exactly as described in Section 4.1. For each simulation, we measure the fraction f_{HDS} and the associated lower and upper confidence limits. The fraction that we finally adopt is the median value of the distribution of f_{HDS} , and the final lower and upper limits are taken as the 68% quantiles of their respective distributions. The final confidence interval is of the same order of the confidence interval when only binomial statistics are considered.

In addition to showing clear evidence for evolution, Figure 8 also shows that the choice of the threshold for $H\delta_A$ does not strongly influence the basic trends seen. We will now show that it is quite straightforward to parameterize f_{HDS} as a function of both redshift and of the threshold $H\delta_{A \text{ min}}$.

At a fixed redshift, f_{HDS} obviously depends on the threshold $H\delta_{A \text{ min}}$. The top panel of Figure 9 presents the histogram of the distribution of $H\delta_A$ for the SDSS galaxies. It is very well fitted by an exponential distribution (a straight line in this log-linear diagram) for $H\delta_A \gtrsim 4 \text{\AA}$: at the median redshift of $z = 0.075$, we have

$$\log_{10} [dN(z)/dH\delta_A] = A(z) + \alpha(z) H\delta_A \quad (1)$$

¹¹ The confidence limits derived using this method are compatible within 4% with the limits computed from the approximate expressions of Gehrels (1986).

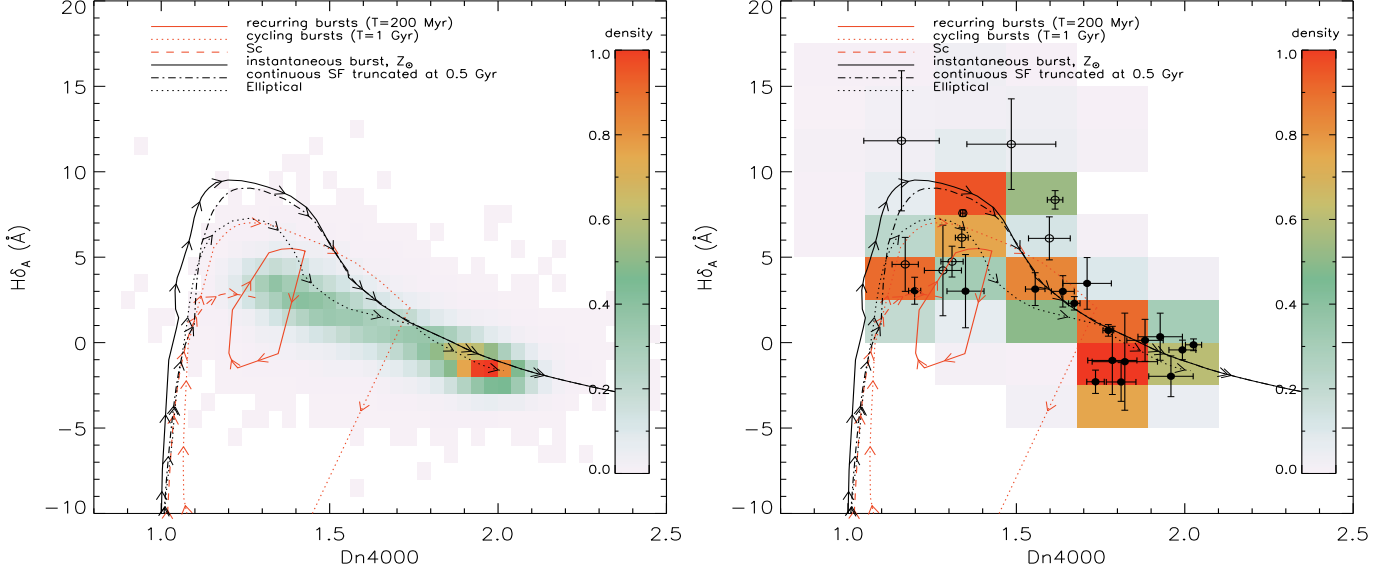


FIG. 6.— Variation of $H\delta_A$ versus D_n4000 for SDSS galaxies (left panel) and GDDS galaxies (right panel). Symbols as in Fig. 3. The arrows on the models (lines) indicate the direction of the evolution. For the ‘cycle’ models (closed loops), only the steady-state cycle (at $z = 0$) is shown, for clarity.

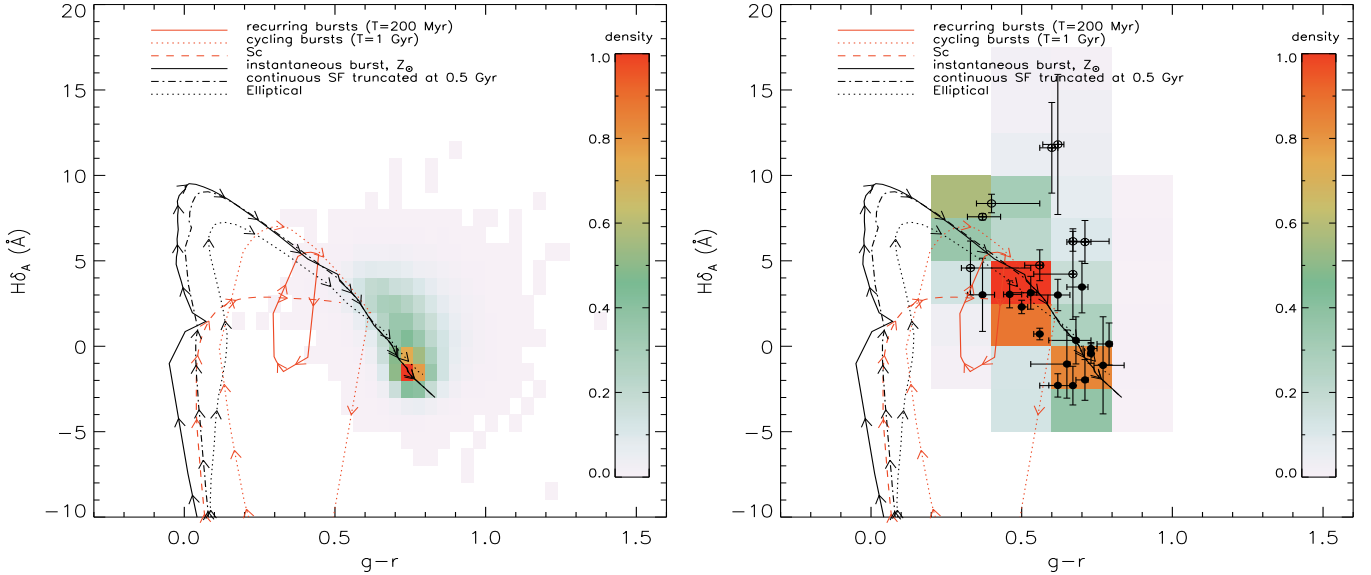


FIG. 7.— Variation of $H\delta_A$ versus $g-r$ rest-frame color for the SDSS sample (left panel) and the GDDS sample (right panel). Symbols as in Fig. 6.

with $\alpha = -0.52$.

We assume in the following that the form of this distribution is still valid at higher redshift. We will show that the data available at $z \approx 1$ is compatible with this assumption.

A distribution of this form should naturally lead to a linear equation for $\log_{10}[f_{\text{HDS}}(H\delta_{A \text{ min}})]$ at a fixed redshift:

$$\log_{10}[f_{\text{HDS}}(z, H\delta_{A \text{ min}})] = \alpha'(z) [H\delta_{A \text{ min}} - H\delta_A^0(z)] \quad (2)$$

with $\alpha' = \alpha$ in the ideal case. $H\delta_A^0(z)$ is introduced here

to account for the offset of this linear equation at the redshift z .

The top panel of Figure 10 shows this quantity f_{HDS} in the SDSS, as a function of the threshold $H\delta_{A \text{ min}}$. As expected, f_{HDS} changes with $H\delta_{A \text{ min}}$ following equation 2, with $\alpha' = -0.53 \approx \alpha$.

At higher redshift, if the distribution of $H\delta_A$ is still an exponential one, then the fraction of HDS galaxies should also follow equation 2. The three bottom panels of Figure 9 present the histograms of the distributions of $H\delta_A$ for GDDS galaxies in the three redshift bins with mean

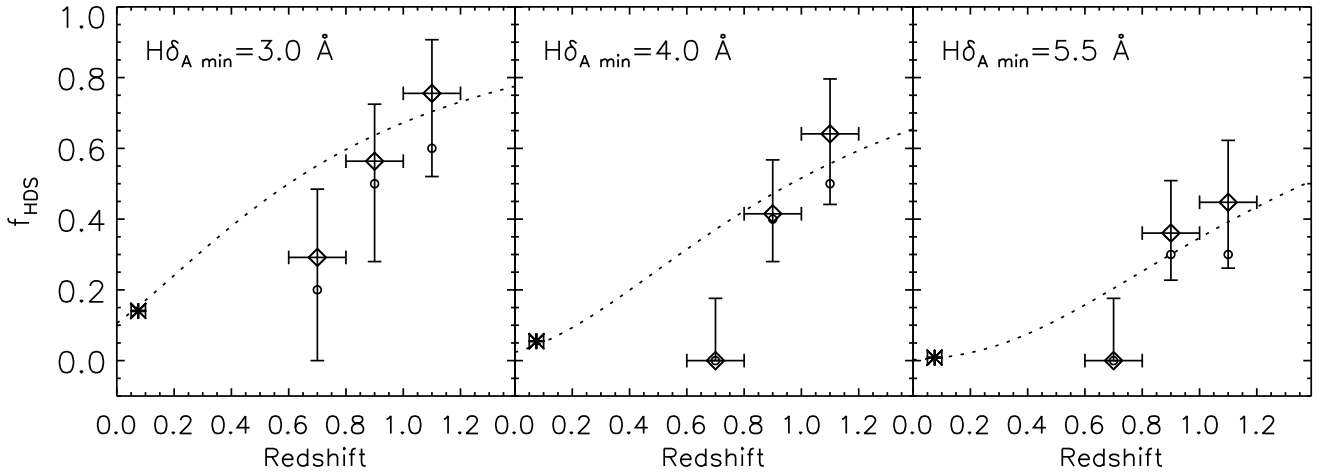


FIG. 8.— Evolution with redshift of the fraction f_{HDS} of $H\delta$ -strong galaxies in populations of massive galaxies. Each panel corresponds to a different threshold for the minimum $H\delta_{\text{A min}}$ value defining HDS galaxies. Triangles represent the SDSS sample. Diamonds and circles represent measurements on the GDDS sample with and without weights, respectively. The increase of f_{HDS} with redshift (roughly, $\log_{10}(f_{\text{HDS}}) \propto -(1+z)^{-2.5}$) corresponds to a $(1+z)^{2.5}$ evolution in the distribution of the $H\delta_{\text{A min}}$ index. The dotted lines illustrate this evolution parameterized by equations 2 and 3 (see text for details).

values $z = 0.7, 0.9$ and 1.1 . These distributions are the results of the Monte-Carlo simulations presented in Section 4, and have an arbitrary normalization. As for the low redshift sample, they seem to be reasonably well described by exponential distributions, with the remarkable point that the slope $\alpha(z)$ increases with redshift. A graphical measure of this increase of $\alpha(z)$ is given in Figure 11 (top panel). We choose to parameterize this evolution by an expression of the form

$$\alpha(z) = k(1+z)^{-m} \quad (3)$$

and we find that $m = 2.0 \pm 1.4$ and $k = -0.6$.

As we said before, if the distribution of $H\delta_{\text{A}}$ remains close to an exponential one at high redshift, the direct measure of f_{HDS} as a function of $H\delta_{\text{A min}}$ should evolve following equation 2. In other words we should find that $\alpha'(z) \approx \alpha(z)$. The two lower panels of Figure 10 present our measurements of f_{HDS} as a function of $H\delta_{\text{A min}}$ for the two highest redshift bins. We observe that at the three redshifts $z \simeq 0.1, 0.9$ and 1.1 , f_{HDS} indeed follows Equation 2, with $H\delta_{\text{A}}^0 \approx 1.5 \text{ \AA}$ in every case. (An explanation for the interesting property that this value seems to be a constant is reserved to further investigation.) Comparing with the previous figure, we do indeed see that $\alpha'(z) \approx \alpha(z)$ in these three redshift bins. Figure 11 (bottom panel) shows the evolution of $\alpha'(z)$, and the best fit is obtained for $m' = 2.5 \pm 0.7$ and $k' = -0.65$, if we use the same form as in equation 3. The values of m and m' are compatible within their error bars but they are slightly different. We can think of two reasons for this (small) difference. Either the distributions of $H\delta_{\text{A}}$ are not really exponentials at high redshift, or the difference is simply due to the smallness of our sample. A larger sample would be useful to refine these values. In any case, if the distribution is indeed an exponential, then we believe that m' , derived from the fits of $f_{\text{HDS}}(z, H\delta_{\text{A min}})$, is actually a more robust number to measure than m , simply because it measures a *cumulative* quantity. The best-fit evolution of f_{HDS} (with the parameters $m' = 2.5$, $k' = -0.65$ and $H\delta_{\text{A}}^0 = 1.5 \text{ \AA}$) is shown explicitly in Figure 8 (dotted lines) and matches the data quite well.

One might notice that the data point for the redshift bin $z = 0.6 - 0.8$ is slightly below the best-fitting idealized curves: in this particular redshift bin, our sample contains only four galaxies, and this small number might not be statistically very significant. Moreover, the proposed parameterization should only be valid for $H\delta_{\text{A min}} \gtrsim 4 \text{ \AA}$, and the left panel of Figure 8 is outside this range, with $H\delta_{\text{A min}} = 3 \text{ \AA}$. Therefore, a good agreement is not expected in this case.

To summarize, we have shown that the fraction of HDS galaxies can be parameterized by equations 2 and 3: f_{HDS} depends both on redshift and on the threshold $H\delta_{\text{A min}}$, but these two variables are independent. In particular, we stress that the evolution of f_{HDS} with redshift does not depend on the threshold $H\delta_{\text{A min}}$ chosen to define HDS galaxies, as long as $H\delta_{\text{A min}} \gtrsim 4 \text{ \AA}$. We have also shown that this evolution of f_{HDS} is a direct consequence of an evolution of the $H\delta_{\text{A}}$ distribution. This distribution is very well described by an exponential distribution at low redshift, and reasonably well in the range $0.8 < z < 1.2$, with an inverse slope $-1/\alpha$ increasing roughly as $\sim (1+z)^{2.5}$. As a result, $\log_{10}(f_{\text{HDS}})$ rises roughly proportionally to $-(1+z)^{-2.5}$, independently of the threshold in $H\delta_{\text{A}}$ that is chosen (if $H\delta_{\text{A min}} \gtrsim 4 \text{ \AA}$). However, we must add an important caveat to this result: the parameterization by Equations 2 and 3 is purely empirical, and constrained only by observations at $z \simeq 0.1$ and $0.8 \lesssim z < 1.2$. Any extrapolation to earlier epochs is hazardous. In particular, these equations suggest a never-ending increase of f_{HDS} with redshift, which is clearly not realistic when the universe is younger than a few 10^8 years and galaxies cannot be in an HDS phase yet.

5. MODELING AND INTERPRETATION

To analyze the observed colors and spectral indices shown in the previous figures, we use the PÉGASE.2 spectral synthesis code (Fioc & Rocca-Volmerange 1997) for broad-band colors and the 4000Å break, together with its version at higher spectral resolution in the optical, PÉGASE-HR (Le Borgne et al. 2004), needed to mea-

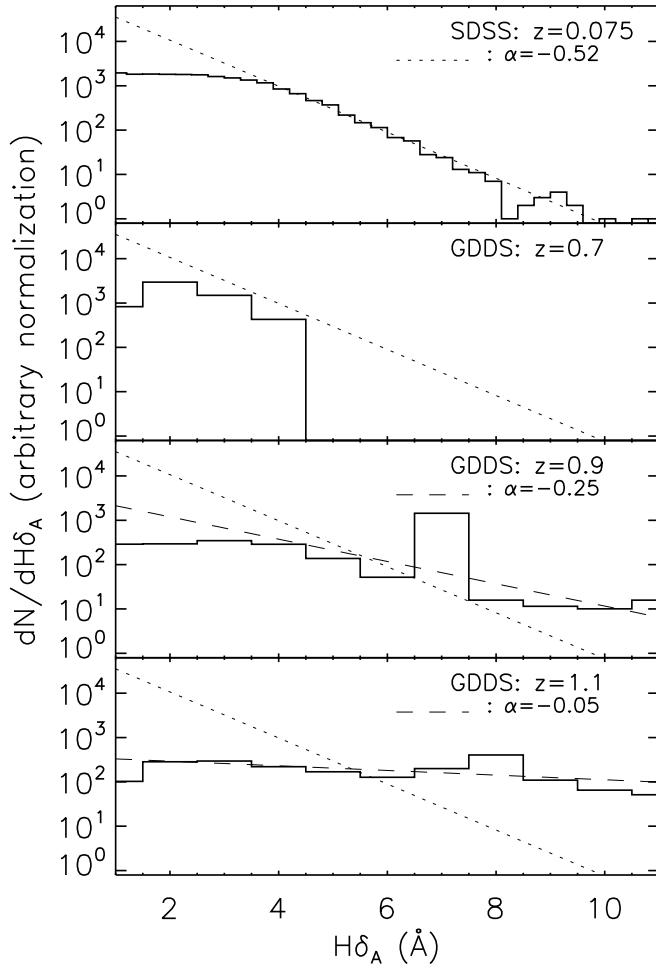


FIG. 9.— Distributions of the $H\delta_A$ index measured in four redshift bins. The slope measured on the SDSS sample (dotted line) for $H\delta_A \gtrsim 4 \text{ \AA}$ is reported in the four panels. For GDSS galaxies, Monte-Carlo simulations were carried out from our sample of 25 galaxies to estimate the real distribution at these redshifts; and the dashed line represents the best-fit pure exponential distribution. The evolution of the slope $\alpha(z)$ is shown in Fig. 11, top panel.

sure Lick indices. The predictions of Lick indices with PÉGASE-HR and their accuracy with respect to other models are fully described in Le Borgne et al. (2004). The differences between the various models available today are small enough to reinforce the robustness of the results in this paper.

In this section, we will compare the observed data with two classes of simple models:

- “Quiescent” models, defined by smooth star formation histories, with continuous and modest star formation rates throughout the life of a galaxy.
- “Burst” models, which correspond to galaxies that build up stellar mass in a few short and intense episodes of star formation.

An archetypal example of a quiescent model is that described by Le Borgne & Rocca-Volmerange (2002) as doing a fairly good job of reproducing the optical and near-infrared colors of local Sc spiral galaxies. In this scenario a galaxy is fed by infall of zero-metallicity gas

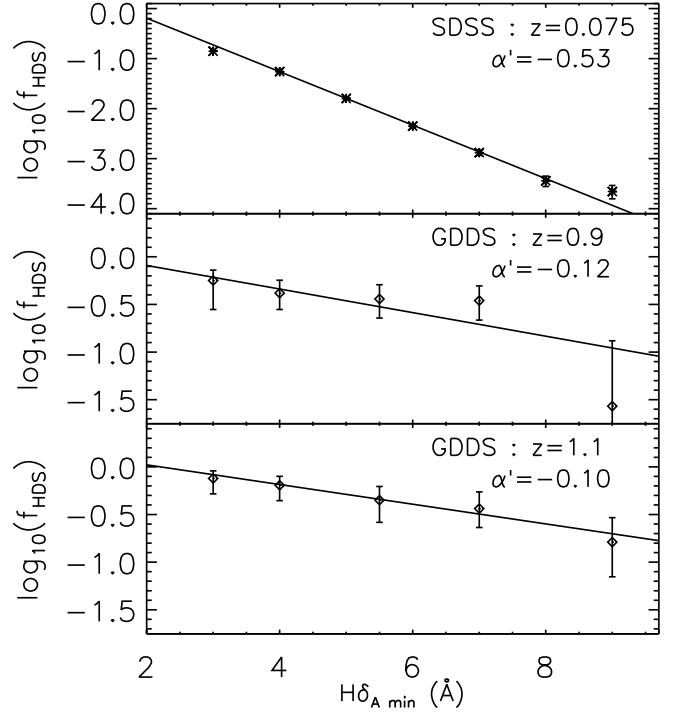


FIG. 10.— Variations of f_{HDS} with the threshold $H\delta_{A \text{ min}}$ for three redshift bins. This figure is directly derived from Fig 9, excluding the bin $0.6 < z < 0.8$ which does not contain enough galaxies to allow a reliable measurement of f_{HDS} . The evolution of the best-fit slope $\alpha'(z)$ is illustrated in Fig. 11, bottom panel.

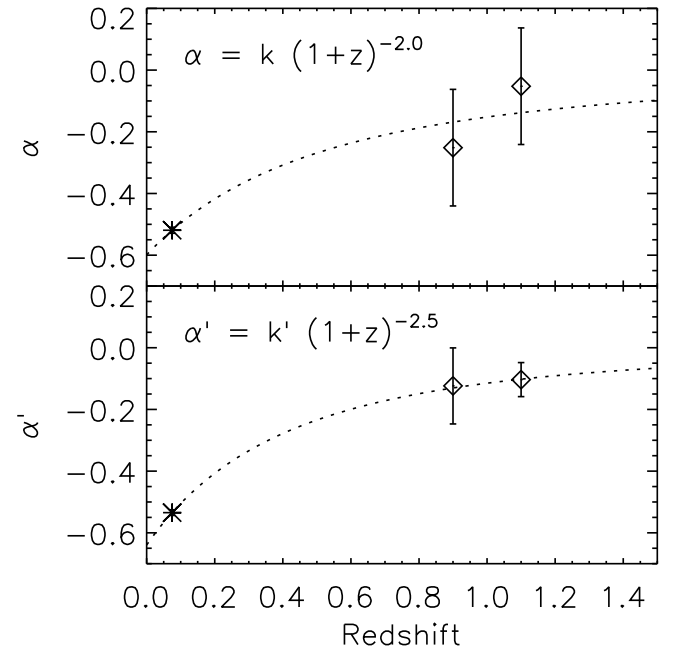


FIG. 11.— Evolutions of the exponential index $\alpha(z)$ of the $H\delta_A$ distribution (top panel) and of the exponential index $\alpha'(z)$ of $f_{\text{HDS}}=f(H\delta_{A \text{ min}})$ (bottom panel). The values of α and α' are reported from Fig. 9 and 10, respectively. In the case of pure exponential distributions for $H\delta_A$ (equation 1), the two panels should be identical.

with a $\tau = 8 \text{ Gyr}$ e-folding time-scale. Inside the galaxy, the gas is simultaneously converted into stars following

a Schmidt law, with a specific efficiency $\nu = 0.1 \text{ Gyr}^{-1}$ ($1/\nu$ being the time required to convert one solar mass of gas into one solar mass of stars). A continuous star formation history can also be approximated by a series of small successive starbursts. The duty cycle of the bursts is encompassed by two evolutionary scenarios, hereafter referred to as “cycling”, or “recurring bursts”. In these models episodic events, which mimic constant star formation, occur during 100 Myr. These are followed by periods of inactivity, lasting 100 Myr in one case (recurring bursts), and 0.9 Gyr in the other case (cycling). It can certainly be argued that our cycling model can hardly be considered to be *continuous* star formation, and in fact it might be better to think of the cycling model as representing a star-formation history that is intermediate between the quiescent mode described here, and the “burst” mode described next.

In contrast to our quiescent models, our burst models are intended to more closely reproduce the colors of local elliptical galaxies. In these models short time-scales ($\nu = \tau = 0.1 \text{ Gyr}$) are associated with the star-formation activity in the first three Gyr. After three Gyr, when the galaxy has converted most of the available gas into stars, galactic winds eject all the remaining gas from the galaxy, preventing further star formation. Two other, more extreme, examples of burst scenarios are a single instantaneous burst with solar metallicity, and a period of constant star formation truncated 0.5 Gyr after the collapse of the galaxy.

Throughout the remainder of this paper we will set a redshift of $z = 1.4$ as the epoch of the last major star formation episode for all the burst-mode models considered. Clearly this redshift does not reflect the real redshift of formation for the galaxies being modeled, which we cannot strongly constrain on account of age-metallicity degeneracy. Instead $z = 1.4$ is simply a fiducial redshift that is supposed to mark roughly the end of the latest major event of active star formation that took place in the HDS massive galaxies. An instantaneous burst model with a redshift of formation $z = 2$ is also considered and shown in Figures 3 and 4, to account for the old and red population of galaxies seen at $z \simeq 1$. In all these models, nebular emission lines are added to the stellar continuum. The fluxes in these lines are computed with PÉGASE.2 for a mean H II region consistently with the on-going and recent star-formation activity in the galaxy. When the star-formation activity is intense, these lines fill-in the absorption stellar lines and often lead to very negative values for the [OII] and H δ equivalent widths.

Tracks corresponding to a representative set of quiescent and burst models are superposed on Figures 3–7. The tracks shown on Figure 3 are particularly illuminating, as these suggest an evolutionary link between the $z = 1$ massive HDS galaxies and the local massive and red galaxies. Indeed, the HDS galaxies that are already massive at $z = 1$ can only be identified as the progenitors of some local massive galaxies: they cannot lose much of their stellar mass (which can be caused by the death of a fraction of the stellar population) during their subsequent evolution. Therefore, the distant HDS galaxies necessarily must be linked to the present massive galaxies, most of which are passively evolving. *It is clear that this evolution can only be modeled by a break in the star-formation history:* the $z \approx 1$ HDS galaxies are

just leaving a burst mode with intense star formation activity (suggested by their already large stellar masses) which ended $\simeq 0.5 - 1 \text{ Gyr}$ before the epoch of observation, at $z \simeq 1.2 - 1.5$. When seen 1-2 Gyr after the burst, at $z \simeq 0.8$, they are evolving almost passively with little star formation, as described in more details below.

We emphasize that the bulk of the massive SDSS galaxies seen at redshift $z = 0.05 - 0.1$ have spectral features characteristic of evolved galaxies with very little star formation activity. Their small H δ_A (Fig. 3), large D_n4000 and red $g - r$ color (Fig. 4) are all well modeled by a passively evolving stellar population, as illustrated by the models shown in Figures 3–7. High-redshift analogs to these objects are seen at $z \sim 1$ in the population of GDDS galaxies marked by solid circles in figures 3. These objects present the same small H δ_A values, large D_n4000 indices, and red $g - r$ colors as evolved galaxies in the local universe¹². These objects connect directly onto a number of recent studies of massive passively evolving galaxies out to even higher redshifts (e.g. McCarthy et al. 2004; Glazebrook et al. 2004; Cimatti et al. 2004).

A comparison of the “quiescent” models (which all have a smoother star-formation history than the burst models) with the data is also interesting. Figure 3 shows that continuous star-formation for a long period of time (Sc model) leads to intermediate values of the H δ_A index ($2 - 3 \text{ \AA}$). This is not true if the star-formation is intermittent: when the star-formation episodes are spaced by more than 100 Myr (which is the case of our recurring and cycle models), the H δ_A index shows substantial variations from very positive (if star-formation is halted abruptly) to very negative values (because of nebular emission lines). The cycle and recurring burst models shown in Figure 4 also make it clear that if the star formation episodes are too frequent (i.e. repeated on periods smaller than a very few Gyrs), the large D_n4000 indices and red rest-frame colors of the massive galaxies at $z = 0$ or $z = 1$ can never be reached.

A particularly nice aspect of modeling H δ_A and D_n4000 is that models used for interpretation of these two quantities are sufficiently robust that uncertainties in them are unlikely to lead to wild misinterpretations of the data. Indeed, we have checked that a change in the IMF, within reasonable limits, does not affect the predicted H δ_A index by more than 2 \AA and D_n4000 by more than 0.2. To some extent, the uncertainties in the stellar evolution tracks can be explored by looking at the differences between the prediction of the PÉGASE models and the Galaxev models (Bruzual & Charlot 2003). Le Borgne et al. (2004) showed that the differences in the predicted H δ_A indices are smaller than 1 \AA at any metallicity. We also verified that the differences on the predicted D_n4000 index are smaller than the errors in the data. However, uncertainties on the effect of the non-solar abundances of α elements remain unclear and might be responsible for slight deviations of the model tracks from the data. The general trends will, however, remain robust.

¹² Note that the stellar mass cutoff we chose when defining our sample corresponds (roughly) to the pivot mass in the observed bimodality between blue and red galaxies in the local universe (Baldry et al. 2004; Kauffmann et al. 2003).

It is worth emphasizing that strong $H\delta$ in absorption is, strictly speaking, a signature of a recent *break* in star-formation, rather than of any preceding star-burst activity. Moreover, a complete halt in the star-formation activity is not needed to obtain an HDS system. It is the contrast between the current and recent-past star-formation rates that must be large.

To illustrate the importance of this contrast, we can show that the current star-formation rate is small in comparison to its average past value by comparing the characteristic growth time-scale of a galaxy to the age of the universe at its redshift. Following Paper V, we define this growth time-scale (expressed in Gyr) as the ratio M_*/SFR : it is the time needed for a galaxy to assemble its current mass if its SFR is fixed at its current value. If the growth time-scale of a galaxy is larger than the age of the universe at its redshift, we can conclude that such a galaxy is in a mode of passive evolution (relative to its past star-formation history). The SFR values of our high redshift galaxies, estimated from the $[OII]\lambda 3727$ emission line and assuming $A_V=1$, are listed in Table 1. The typical values of the on-going SFR are $1-2 M_\odot \text{ yr}^{-1}$ for HDS galaxies (and $0.1 - 1 M_\odot \text{ yr}^{-1}$ for the non-HDS, “older” galaxies). Although these values are non negligible, they are still small with respect to the past mean SFR: Table 1 shows that M_*/SFR is larger than the age of the universe, in a ratio of $\simeq 3$ for the HDS galaxies, and $\simeq 10$ for the non-HDS galaxies. This is in good agreement with the results of Paper V, and it means that the massive galaxies are already in a mode of passive evolution at $z = 1$. It also illustrates the large contrast between the recent ($\simeq 1$ Gyr ago) large bursts of star formation and the modest values of the on-going SFR in HDS systems.

The classical way to study “post-starburst” galaxies (i.e. with completely truncated star formation) is to focus on the sub-sample of HDS galaxies with little (or no) emission lines, as measured by their equivalent widths. The most well-known categorization of these galaxies is the ‘E+A’ population (Dressler & Gunn 1983; Balogh et al. 1999; Poggianti et al. 1999; Zabludoff et al. 1996), with strong $H\delta$ absorption lines coupled with little (or no) $[OII]$ emission. To facilitate comparison with previous work, we conclude this section by investigating the fraction of ‘E+A’ galaxies in our HDS population. Table 1 includes measurements of $[OII]$ equivalent width, with emission lines represented by negative values¹³. As described below, our GDDS sample contains one or two E+A galaxies, depending on how error bars are treated.

Figure 12 shows the distribution of the two samples of massive galaxies on a $EW(H\delta)$ - $EW[O II]$ diagram. The SDSS sample is represented with the same color-coding of the number density as in previous figures. The individual GDDS galaxies are shown with their error bars. Some very simple closed-box evolutionary models computed with PÉGASe are over-plotted: these models have exponentially decreasing star-formation rates with e-folding time-scales $\tau = 3, 10, 100, 200$ and 1000 Myr (Column 1

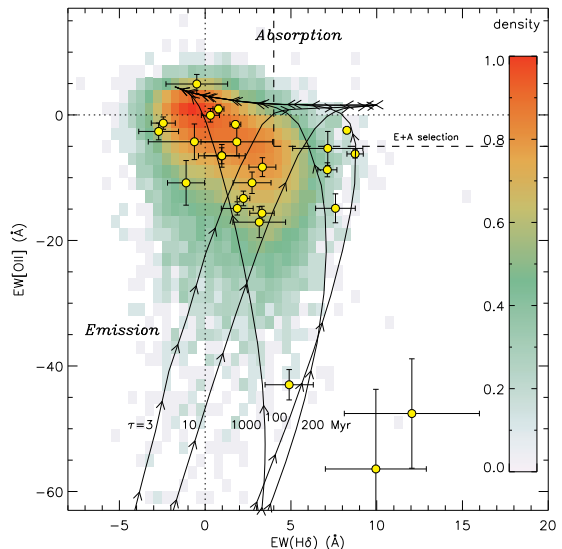


FIG. 12.— Selection of E+A galaxies (defined by the dashed box: $EW(H\delta) > 4 \text{ \AA}$ and $EW[O II] > -5 \text{ \AA}$). The shaded colored region corresponds to the SDSS sample (same color-coding as in Fig. 3). The individual GDDS galaxies of our sample are shown on the top of the SDSS sample, with their error bars. The evolutions predicted by closed-box exponential models (solid lines, with arrows marking every doubling in age) are given for various e-folding time-scales τ . The fraction of galaxies in the E+A phase (or simply in the HDS phase with $EW(H\delta) > 4 \text{ \AA}$) is much larger in the GDDS sample than at low redshift. Moreover, only models corresponding to a rapid decrease of the star-formation rate ($\tau \lesssim 300$ Myr) reach the E+A phase (see also Table 3).

TABLE 3
CLOSED-BOX MODELS WITH EXPONENTIALLY DECREASING SFR.

τ (Gyr)	$EW(H\delta)$ (\AA)	Age (Gyr)	Δt_{HDS} (Gyr)	$\Delta t_{\text{E+A}}$ (Gyr)
0.003	10.0	0.25	1.56	1.56
0.01	10.0	0.30	1.54	1.53
0.1	8.8	0.60	1.48	1.11
0.2	7.1	0.80	1.51	0.67
1.0	3.5	1.80	0.00	0.00

of Table 3). All these models form stars at solar metallicity. The arrows give the direction of the evolution in the diagram: $EW[O II]$ is highly negative soon after the maximum of the star formation because of the presence of strong emission lines, and increases continuously afterward. The models with $\tau < 300$ Myr pass through an HDS phase (if defined by $EW(H\delta) > 4 \text{ \AA}$) and an E+A phase (if defined by an HDS galaxy with $EW[O II] > -5 \text{ \AA}$) which is illustrated by the dashed line in Figure 12.

The maximum $EW(H\delta)$ values reached by our models, and the corresponding ages, are given in Table 3, Columns 2 and 3. This table also records (Columns 4 and 5) the total time spent in the HDS and E+A phases. The table shows that (i) the maximum $EW(H\delta)$ is reached sooner for rapidly decreasing SFRs, (ii) the time spent in the HDS phase is almost independent of the e-folding time-scale when this phase is reached, and (iii) a given galaxy spends less time in the E+A phase when the SFR declines more slowly. On this basis, it is clear from Figure 12 that the proportion of galaxies show-

¹³ Note that, for this analysis, we chose to use the definition of the equivalent width $EW(H\delta)$ given in Table 2 instead of the Lick $H\delta_A$ index used earlier in this paper in order to make our results directly comparable to previous work (Abraham et al. 1996; Balogh et al. 1999; Goto et al. 2003; Tran et al. 2004). When measured on the SDSS sample, the average value of $EW(H\delta) - H\delta_A$ is 0.50 \AA , with an rms dispersion of 0.78 \AA .

ing signs of recently truncated star formation ($\tau < 200$ Myr and $\text{EW}(\text{H}\delta) > 4 \text{ \AA}$) is higher for the GDDS sample than for the SDSS sample.

Models in Table 3 and Figure 12 can be used to make a theoretical prediction regarding the evolution of E+A systems: while models with $\tau < 300$ Myr have both an HDS and an E+A phase, all models that have an HDS phase do not necessarily have a E+A phase. (For instance, models with $0.3 < \tau < 1.0$ Gyr). Therefore, depending on how fast the star-formation is halted, one might expect that the evolution of the fraction of E+A galaxies would show milder evolution than the fraction of HDS galaxies. Strictly speaking, $4_{-3}^{+5}\%$ (1/25) of the GDDS galaxies are E+A at $z = 0.6 - 1.2$ and 3.1% (1561/50,255) of the SDSS sample at $z = 0.05 - 0.1$ meet the E+A definition. (The GDDS galaxy 02-1543 might be counted as an additional E+A, depending on how one treats its error bar.) The fractions at low and high redshifts being roughly compatible, we don't observe any evolution in the fraction of E+A galaxies. However, the small number statistics involved and our large error bars leave room for further studies on this topic.

It is of interest to note that a number of recent papers derive a $(1+z)^m$ evolution to describe the rise in the merger rate as a function of redshift, with m indices that are similar to the exponential index we obtain for the rise in the fraction of HDS systems as a function of redshift: compare our value of $m = 2.5 \pm 0.7$ with $m = 3.4 \pm 0.6$ obtained by Le Fèvre et al. (2000) and $m = 2.5 \pm 0.7$ obtained by Patton et al. (2002). However, the evolution in the merger rate is poorly constrained. For example, larger values are also obtained, such as $m = 4 \pm 1$ by Reshetnikov (2000) and $m = 4 - 6$ according to Conselice et al. (2003). At this stage we think the most that can be said is that our results may hint at a relationship between merging and the HDS phase. A similar relationship is suggested by the recent work of Goto (2005) on 266 E+A galaxies in the SDSS. If a link exists between HDS galaxies and mergers, the morphologies of HDS galaxies should reflect these dramatic events. Figure 1 shows that many of the HDS galaxies (left column) indeed have disturbed morphologies which can be signs of merging. Moreover, the ratio between irregular and relaxed morphologies should roughly scale as the ratio of time-scales for merging ($\simeq 0.5$ Gyr) and spectral evolution ($\simeq 0.3 - 2$ Gyr). This statement seems generally consistent with Figure 1, which shows several HDS galaxies with almost relaxed morphologies (02-1724, 02-1777, 22-0315), but further discussion of this topic is reserved for an upcoming paper in this series (Abraham et al. 2006, in preparation).

6. CONCLUSIONS

By comparing two mass-selected samples of galaxies at low (SDSS) and high (GDDS) redshift, we find that the fraction of galaxies with strong H δ absorption lines increases with redshift up to $z = 1.2$. This evolution can be parameterized as a function of redshift: $(1+z)^{2.5 \pm 0.7}$. It does not depend on the threshold chosen for H δ_A to define HDS galaxies, and it reflects a similar evolution for the distributions of the H δ equivalent widths. By modeling this variation using PÉGASE models as a function of D_n4000 and the rest-frame $g-r$ color, we conclude that this evolution originates from a fundamental change in

the mode of star formation in massive galaxies that occurred somewhere around $z \simeq 1.4 - 2$. Our models suggest that the star formation rates drop sharply in most massive galaxies at that epoch, which is consistent with the measures of star formation rate densities presented in Paper V.

This drop in the star formation rate, together with the already large stellar masses of these $z \simeq 1$ galaxies, suggests very active phases in the star-formation at higher redshifts. The massive obscured starbursts being detected with the Spitzer Space Telescope at $z \simeq 2 - 2.5$ could very well be the progenitors of our sample of $z \simeq 1$ galaxies: the "old" galaxies seen in our sample at $z = 1$, with small H δ_A indices and large D_n4000 breaks, have necessarily experienced their last significant episodes of star-formation at $z \gtrsim 1.8$ and assembled most of their stellar mass before that time. These episodes must have been very intense (at least $\simeq 30 M_\odot \text{ yr}^{-1}$ on average), given the large stellar mass of these galaxies and the age of the universe at this redshift. Moreover, some of the $z = 2 - 2.5$ starbursts could also have spanned larger timescales (2 - 3 Gyr) in which case they could become HDS galaxies at $z \simeq 1$, on the condition that their star-formation declined at $z \simeq 1.4$, on time-scales shorter than a few hundred Myrs. This picture is in fairly good agreement with the recent findings of Treu et al. (2005) who estimate that the massive field spheroidal galaxies seen at $z = 0.2 - 1.2$ in the GOODS-N field formed most of their stellar mass at $z \gtrsim 2$, with subsequent activity continuing to lower redshifts.

Finally, our study of spectral features in massive galaxies from $z = 1.2$ to the present shows that the redshift range $z = 1.4 - 2$ corresponds to the epoch at which the star-formation in these galaxies has changed from an active phase to a passive one. An echo of this change in the mode of star-formation activity is imprinted in the strong H δ absorption lines seen in massive galaxies at $z \sim 1$.

7. ACKNOWLEDGMENTS

The authors wish to thank Jarle Brinchmann for many stimulating discussions and for sharing with us a number of plots which motivated much of this work. We are also in debt to the anonymous referee whose comments helped to improve the quality of this paper. Observations were obtained at the Gemini Observatory, which is operated by AURA Inc., under a cooperative agreement with the NSF on behalf of the Gemini partnership: the NSF (US), PPARC (UK), NRC (Canada), CONICYT (Chile), ARC (Australia), CNPq (Brazil) and CONICET (Argentina) and at the Las Campanas Observatory of the OCIW. RGA acknowledges support from NSERC and the Province of Ontario. KG and SS acknowledge support from the David and Lucille Packard Foundation. Funding for the creation and distribution of the SDSS Archive has been provided by the Alfred P. Sloan Foundation, the Participating Institutions, the National Aeronautics and Space Administration, the National Science Foundation, the U.S. Department of Energy, the Japanese Monbukagakusho, and the Max Planck Society. The SDSS Web site is <http://www.sdss.org/>. The SDSS is managed by the Astrophysical Research Consortium (ARC) for the Participating Institutions. The Participating Institutions are The University of Chicago,

Fermilab, the Institute for Advanced Study, the Japan Participation Group, The Johns Hopkins University, the Korean Scientist Group, Los Alamos National Laboratory, the Max-Planck-Institute for Astronomy (MPIA), the Max-Planck-Institute for Astrophysics (MPA), New

Mexico State University, University of Pittsburgh, University of Portsmouth, Princeton University, the United States Naval Observatory, and the University of Washington.

REFERENCES

- Abazajian, K., Adelman-McCarthy, J. K., Agüeros, M. A., et al. 2004, *AJ*, 128, 502
- Abraham, R. G., Glazebrook, K., McCarthy, P. J., et al. 2004, *AJ*, 127, 2455 [Paper I]
- Abraham, R. G., Smecker-Hane, T. A., Hutchings, J. B., et al. 1996, *ApJ*, 471, 694
- Abraham, R. G. et al. 2006, *AJ*, in prep.
- Baldry, I. K. & Glazebrook, K. 2003, *ApJ*, 593, 258
- Baldry, I. K., Glazebrook, K., Brinkmann, J., et al. 2004, *ApJ*, 600, 681
- Balogh, M. L., Morris, S. L., Yee, H. K. C., Carlberg, R. G., & Ellingson, E. 1999, *ApJ*, 527, 54
- Bell, E. F., et al. 2004, *ApJ*, 608, 752
- Blanton, M. R., et al. 2003, *ApJ*, 592, 819
- Brinchmann, J., Charlot, S., White, S. D. M., et al. 2004, *MNRAS*, 351, 1151
- Bruzual, G. & Charlot, S. 2003, *MNRAS*, 344, 1000
- Cardiel, N., Gorgas, J., Cenarro, J., & Gonzalez, J. J. 1998, *A&AS*, 127, 597
- Chen, H., McCarthy, P. J., Marzke, R. O., et al. 2002, *ApJ*, 570, 54
- Cimatti, A., Daddi, E., Renzini, A., et al. 2004, *Nature*, 430, 184
- Cole, S., et al. 2001, *MNRAS*, 326, 255
- Conselice, C. J., Bershady, M. A., Dickinson, M., & Papovich, C. 2003, *AJ*, 126, 1183
- Couch, W. J. & Sharples, R. M. 1987, *MNRAS*, 229, 423
- Dressler, A. & Gunn, J. E. 1983, *ApJ*, 270, 7
- Dressler, A. & Shectman, S. A. 1987, *AJ*, 94, 899
- Fasano, G., & Franceschini, A. 1987, *MNRAS*, 225, 155
- Fioc, M. & Rocca-Volmerange, B. 1997, *A&A*, 326, 950
- . 1999, *astro-ph/9912179*
- Firth, A. E., Somerville, R. S., McMahon, R. G., et al. 2002, *MNRAS*, 332, 617
- Fontana, A., Pozzetti, L., Donnarumma, I., et al. 2004, *A&A*, 424, 23
- Gehrels, N. 1986, *ApJ*, 303, 336
- Glazebrook, K., Abraham, R. G., McCarthy, P. J., et al. 2004, *Nature*, 430, 181 [Paper III]
- Goto, T. 2005, *MNRAS*, 357, 937
- Goto, T., Nichol, R. C., Okamura, S., et al. 2003, *PASJ*, 55, 771
- Juneau, S., Glazebrook, K., Crampton, D., et al. 2005, *ApJ*, 619, L135 [Paper V]
- Kauffmann, G., Heckman, T. M., White, S. D. M., et al. 2003, *MNRAS*, 341, 33
- Kewley, L. J., Geller, M. J., & Jansen, R. A. 2004, *AJ*, 127, 2002
- Kroupa, P. 2001, *MNRAS*, 322, 231
- Le Borgne, D. & Rocca-Volmerange, B. 2002, *A&A*, 386, 446
- Le Borgne, D., Rocca-Volmerange, B., Prugniel, P., et al. 2004, *A&A*, 425, 881
- Le Fèvre, O., Abraham, R., Lilly, S. J., et al. 2000, *MNRAS*, 311, 565
- Madau, P., Pozzetti, L., & Dickinson, M. 1998, *ApJ*, 498, 106
- McCarthy, P. J., Carlberg, R. G., Chen, H.-W., et al. 2001, *ApJ*, 560, L131
- McCarthy, P. J., Le Borgne, D., Crampton, D., et al. 2004, *ApJ*, 614, L9 [Paper IV]
- Panter, B., Heavens, A. F., & Jimenez, R. 2004, *MNRAS*, 458
- Paterno, M. 2004, Calculating Efficiencies and their Uncertainties, Tech. Rep. FERMILAB-TM-2286-CD, Fermilab Technical Memo, see also <http://home.fnal.gov/~paterno/images/effic.pdf>
- Patton, D. R., Pritchett, C. J., Carlberg, R. G., et al. 2002, *ApJ*, 565, 208
- Poggianti, B. M., Smail, I., Dressler, A., et al. 1999, *ApJ*, 518, 576
- Quintero, A. D., Hogg, D. W., Blanton, M. R., et al. 2004, *ApJ*, 602, 190
- Reshetnikov, V. P. 2000, *A&A*, 353, 92
- Salpeter, E. E. 1955, *ApJ*, 121, 161
- Schmidt, M. 1968, *ApJ*, 151, 393
- Shioya, Y., Bekki, K., & Couch, W. J. 2004, *ApJ*, 601, 654
- Tran, K. H., Franx, M., Illingworth, G. D., et al. 2004, *ApJ*, 609, 683
- Treu, T., et al. 2005, *ApJ*, 633, 174
- Worthey, G. & Ottaviani, D. L. 1997, *ApJS*, 111, 377
- Yang, Y., Zabludoff, A. I., Zaritsky, D., Lauer, T. R., & Mihos, J. C. 2004, *ApJ*, 607, 258
- Zabludoff, A. I. 1999, in *IAU Symp. 186: Galaxy Interactions at Low and High Redshift*, 125
- Zabludoff, A. I., Zaritsky, D., Lin, H., et al. 1996, *ApJ*, 466, 104